

Magnetic Properties of  $\text{Ga}_{2-x}\text{Fe}_x\text{O}_3$ †

B. F. LEVINE,\* C. H. NOWLIN,‡ AND R. V. JONES

*Gordon McKay Laboratory, Harvard University, Cambridge, Massachusetts*

(Received 5 March 1968)

The experimental dependence of the magnetization on temperature and composition is presented for  $\text{Ga}_{2-x}\text{Fe}_x\text{O}_3$ . Interpretation is based on a three-sublattice model, giving the  $x$  dependence of the iron occupation of the various sites, the variation of the Curie temperature with  $x$ , and the molecular-field coefficients  $\lambda_{ij}$ . These results permit a dipolar anisotropy calculation of the anisotropy constants as a function of temperature and  $x$  in good agreement with experiment. The dipolar contribution to the magnetoelastic energy is also calculated.

## I. INTRODUCTION

THE orthorhombic phase of the compound  $\text{GaFeO}_3$  is unique in that it is the only currently known piezoelectric material which has an appreciable spontaneous magnetic moment. Since it also has a very large magnetoelectric interaction, this material has generated considerable interest in several laboratories. For brevity, we will identify the piezoelectric-ferromagnetic phase of  $\text{GaFeO}_3$  by the acronym MEGIO for magnetoelectric gallium iron oxide. An earlier paper<sup>1</sup> reported some preliminary magnetic data on mixed MEGIO crystals. In this paper, we present a more complete experimental picture of the magnetic properties of these crystals and attempt to interpret their properties in terms of the recently determined crystal and magnetic structures of the compound.

Remeika<sup>2</sup> first prepared MEGIO in 1959, apparently in conjunction with a study of the structure of  $\beta$   $\text{Ga}_2\text{O}_3$ . He discovered that powders characterized by a compositional formula  $\text{Ga}_{2-x}\text{Fe}_x\text{O}_3$  ( $0.7 \leq x \leq 1.4$ ) exhibited a new orthorhombic, piezoelectric crystal structure and a net spontaneous magnetic moment. Remeika also devised a flux method for growing small but high quality single crystals of this new material. Wood<sup>3</sup> measured the unit-cell dimensions of the phase and determined its space group to be  $Pc2_1n(C_{2v}^9)$ , ( $c < a < b$ ). Since 1960, a number of properties of MEGIO have been measured in considerable detail. In particular, some interesting magnetoelectric effects have been reported by Rado.<sup>4</sup> However, until recently, any complete theoretical interpretation of these various properties has been greatly hampered by the lack of both a crystal-structure determination and an adequate

model of the magnetic structure. Because of the work of Abrahams *et al.*<sup>5</sup> and Bertaut *et al.*<sup>6</sup> a complete, precise three-dimensional crystal structure is now available. The neutron-diffraction and magnetic measurements of Bertaut *et al.*<sup>7</sup> have greatly clarified the magnetic structure, as have high-field Mössbauer studies by Frankel *et al.*<sup>8</sup>

In Sec. II of this paper we present the results of magnetic measurements on single crystals of MEGIO for several values of  $x$ . These results represent a more complete version of preliminary data presented in an earlier paper.<sup>1</sup> The magnetic properties of MEGIO are extremely anisotropic with the total magnetic moment oriented along the  $c$  or "needle" axis of the crystals by an anisotropy field of order  $10^6$  Oe. The temperature variation of the spontaneous magnetization along the  $c$  axis follows a nearly classical "Brillouin-like" behavior. For the particular case of  $x=1$ , the low-temperature spontaneous moment is 0.76 Bohr magnetons per ferric ion and the ordering temperature is 240°K.

The interpretation of these data and other known magnetic properties in terms of the crystal structure of MEGIO is given in Sec. III. It is shown that all of the magnetic measurements are consistent with a molecular-field treatment of the three-sublattice ferrimagnetic model of Bertaut *et al.*<sup>6,7</sup> A statistical argument is used to account for the stoichiometric variations in the spontaneous moment and Curie temperature.

In Sec. IV we present the results of a molecular-field calculation of the classical dipolar energy of the MEGIO lattice. The dipolar energy is sufficient to account for the magnitude, sign, temperature variation, and iron concentration dependence of the large magnetocrystalline anisotropy of MEGIO. The dipolar contribution to the magnetoelastic constants is also presented.

† Research supported in part by the Office of Naval Research, Contract No. N00014-67-A-0298-0006, and Office of Aerospace Research AFRL Contract No. AF 19(628) 3874.

\* National Science Foundation Predoctoral Fellow.

‡ Present address: Oak Ridge National Laboratory, Oak Ridge, Tenn.

<sup>1</sup> C. H. Nowlin and R. V. Jones, *J. Appl. Phys.* **34**, 1262 (1963).

<sup>2</sup> J. P. Remeika, *J. Appl. Phys.* **31**, 2635 (1960).

<sup>3</sup> E. A. Wood, *Acta Cryst.* **13**, 628 (1960).

<sup>4</sup> G. T. Rado, *Phys. Rev. Letters* **13**, 335 (1964); *J. Appl. Phys.* **37**, 1403 (1966).

<sup>5</sup> S. C. Abrahams, J. M. Reddy, and J. L. Bernstein, *J. Chem. Phys.* **42**, 3957 (1965).

<sup>6</sup> E. F. Bertaut, G. Buisson, J. Chappert, and G. Bassi, *Compt. Rend.* **260**, 3355 (1965).

<sup>7</sup> E. F. Bertaut, G. Bassi, G. Buisson, J. Chappert, A. Delapalme, R. Pauthenet, H. P. Reboiillat, and R. Aleonard, *J. Phys. (Paris)* **27**, 433 (1966).

<sup>8</sup> R. B. Frankel, N. A. Blum, S. Foner, A. J. Freeman, and M. Schieber, *Phys. Rev. Letters* **15**, 958 (1965).

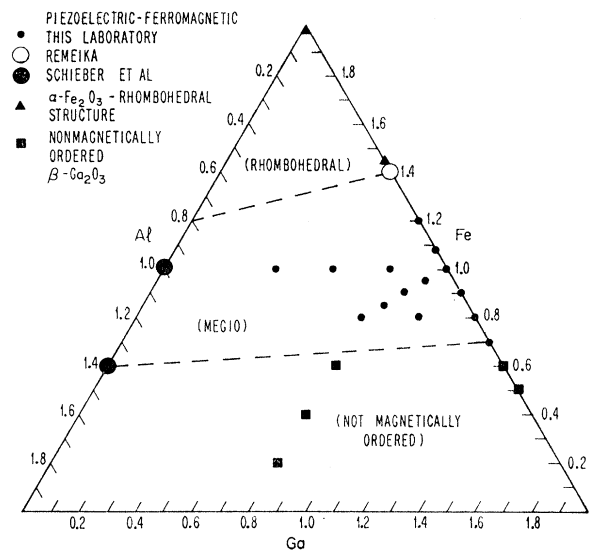


FIG. 1. The ternary diagram for the  $\text{Al}_2\text{O}_3$ - $\text{Fe}_2\text{O}_3$ - $\text{Ga}_2\text{O}_3$  system.

## II. EXPERIMENTAL

### A. Crystal System

Magnetic-moment measurements have been made on a representative group of small ( $\approx 5$  mg) single-crystal samples of MEGIO which were grown in our laboratory using Remeika's<sup>2</sup> bismuth-oxide-boron-oxide flux technique. The relative cation concentrations of these samples span the entire range of the iron-gallium ratios over which we were able to grow good quality crystals, i.e.,  $0.8 \leq x \leq 1.1$  in the chemical formula  $\text{Ga}_{2-x}\text{Fe}_x\text{O}_3$ . Remeika was able to prepare MEGIO powder over the somewhat wider range  $0.7 \leq x \leq 1.4$ .

In an attempt to grow a paramagnetic host crystal isomorphic to MEGIO, various aluminum-containing samples were also grown. A ternary diagram, Fig. 1, indicates the various chemical compositions of the crystals which were tried. Also indicated are the estimated boundaries for the stability of the orthorhombic piezoelectric ferromagnetic phase. The lines are dotted since the boundaries for the aluminum-rich region of the MEGIO phase are more uncertain than for the gallium-rich end.

For  $x$  above the boundary ( $x > 1.4$  for pure  $\text{Ga}_{2-x}\text{Fe}_x\text{O}_3$ )

TABLE I. Basic information on the samples studied most intensively.

Chemical composition of the starting melt	Crystal composition by microchemical analysis	Magnetic moment in Bohr magnetons per ferric ion at 4.2°K and 6537 Oe
$\text{Ga}_{1.3}\text{Fe}_{0.7}\text{O}_3$	$\text{Ga}_{1.18}\text{Fe}_{0.82}\text{O}_3$	0.395
$\text{Ga}_{1.2}\text{Fe}_{0.8}\text{O}_3$	$\text{Ga}_{1.14}\text{Fe}_{0.86}\text{O}_3$	0.540
$\text{Ga}_{1.1}\text{Fe}_{0.9}\text{O}_3$	$\text{Ga}_{1.07}\text{Fe}_{0.93}\text{O}_3$	0.630
$\text{Ga}_{1.0}\text{Fe}_{1.0}\text{O}_3$	$\text{Ga}_{0.98}\text{Fe}_{1.02}\text{O}_3$	0.789
$\text{Ga}_{0.92}\text{Fe}_{1.08}\text{O}_3$	$\text{Ga}_{0.89}\text{Fe}_{1.11}\text{O}_3$	0.935
$\text{Ga}_{0.8}\text{Al}_{0.2}\text{Fe}_{1.0}\text{O}_3$	$\text{Ga}_{0.81}\text{Al}_{0.11}\text{Fe}_{1.09}\text{O}_3$	0.793

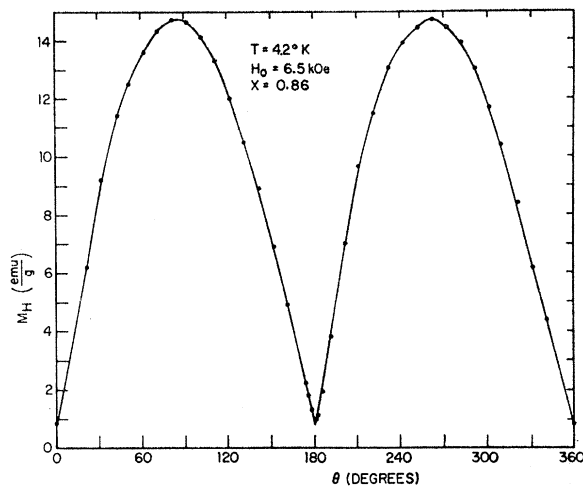


FIG. 2. Magnetization rotation curve in  $bc$  plane for  $\text{Ga}_{1.14}\text{Fe}_{0.86}\text{O}_3$ .  $\theta$  is the angle between the  $b$  axis and the external field  $H_0$ .  $M_H$  is the component of  $M$  along  $H_0$  (measured by K. Kritayakirana).

we find the iron-rich compounds of  $\text{Ga}_{2-x}\text{Al}_y\text{Fe}_z\text{O}_3$  have the rhombohedral  $\alpha$ - $\text{Fe}_2\text{O}_3$  structure, while, if  $x$  is below the boundary ( $x < 0.7$  for pure  $\text{Ga}_{2-x}\text{Fe}_x\text{O}_3$ ), it results in a nonmagnetically ordered state (monoclinic  $\beta$   $\text{Ga}_2\text{O}$  at the gallium-rich end). The structures of all samples were checked by the use of a Weissenberg rotating-sample x-ray camera. Schieber *et al.*<sup>9</sup> have grown orthorhombic  $\text{Al}_{2-x}\text{Fe}_x\text{O}_3$  for the approximate range  $0.6 < x < 1$  and find the aluminum-rich  $\text{Al}_{2-x}\text{Fe}_x\text{O}_3$  to be rhombohedral.

The compositions plotted in Fig. 1 are those determined by the relative amounts of the various starting materials rather than by chemical analysis of the resulting crystals. The difference between these determinations is indicated in Table I. For the samples used

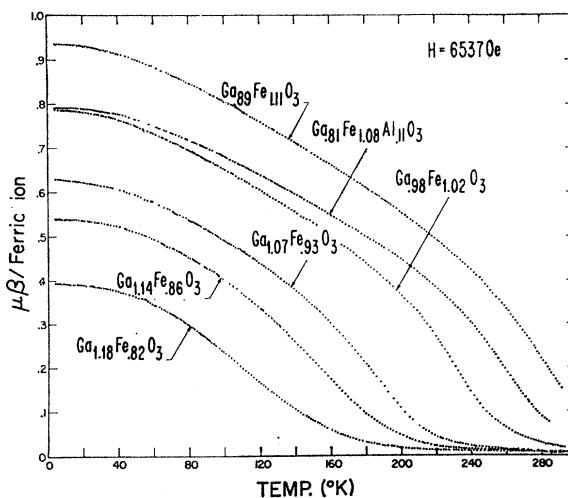
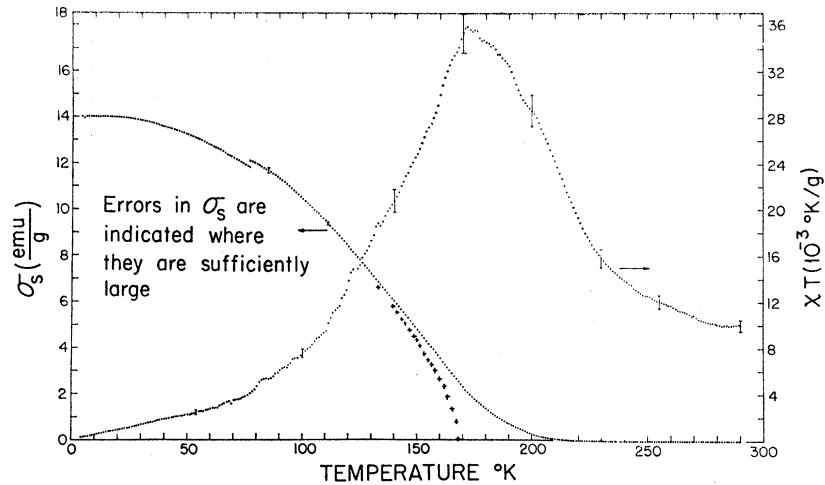


FIG. 3. Finite-field magnetic moment of  $\text{Ga}_{2-x}\text{Fe}_x\text{O}_3$  versus temperature.

<sup>9</sup> M. Schieber, R. B. Frankel, N. A. Blum, and S. Foner, *J. Appl. Phys.* **38**, 1282 (1967).

FIG. 4. Spontaneous magnetization and susceptibility-temperature product along the  $c$  axis of  $\text{Ga}_{1.14}\text{Fe}_{0.86}\text{O}_3$ . The artificial break at 77°K is discussed in the text. The points marked with + are thermodynamically redetermined magnetization.



in the magnetic measurements, the values of  $x$  and  $y$  were measured to within 2% by microchemical analysis.

The relatively horizontal MEGIO phase boundaries indicate that the aluminum is being substituted in the crystal for gallium rather than iron. The preference of aluminum and gallium for the same crystal sites is consistent with the substitutional behavior of these ions in other magnetic oxides.<sup>10</sup>

Because of smallness of the available crystals, even small pockets of flux or voids could be the source of appreciable error in the measured magnetic moment. However, samples having high acoustical  $Q$ 's (comparable to quartz), as measured in a marginal-oscillator piezoelectric detector, proved to have a negligible amount of such defects. Only such high- $Q$  samples were used for the measurements.

### B. Magnetization Curves

The magnetic moments of the small MEGIO crystals were measured by means of a Foner-type vibrating-sample magnetometer. The magnetometer had an ultimate sensitivity of approximately  $3 \times 10^{-6}$  cgs emu, which made possible the detection of very small variations in the moments of our minuscule samples ( $\approx 5$  mg) even at temperatures somewhat above the ordering temperature. The details of the magnetometer are discussed in an unpublished report.<sup>11</sup>

A typical magnetization rotation curve of MEGIO is shown in Fig. 2. As is evident, the material is extremely anisotropic. The total magnetic moment is strongly constrained to be oriented nearly parallel to the  $c$  axis of the orthorhombic cell. The  $c$  axis is the "needle" axis of the characteristic growth habit of the MEGIO crystals. For magnetic fields along the  $c$  axis and at values above the domain saturation "knee," the field-dependent moment per gram fits quite well an expres-

sion of the form

$$\sigma(H, T) = \sigma_0(T) + \chi_c(T)H, \quad (1)$$

where  $\sigma_0(T)$  is the extrapolated zero-field moment. Unfortunately, our experiments were limited to a maximum field of 7.0 kOe. Within this range, however, the magnetization curves showed no tendency towards saturation. It has been found<sup>8</sup> that Eq. (1) remains valid at extremely high magnetic fields.

Since MEGIO has such a large magnetocrystalline anisotropy, shape anisotropy effects were of little importance. Spherical and prismatic samples yielded indistinguishable results. Hence, in general, spherical samples were not used and the growth habit of the crystal was a valuable aid in crystal orientation.

These results may be understood if we assume that the magnetization is strongly held to the  $c$  axis and only small field-induced misalignments are possible. Since we measure the projection of moment along the direction of  $\mathbf{H}$ , the measured moment should follow a curve

$$\sigma_{\text{meas}} = \sigma_s \cos\theta + \sigma_s \sin^2\theta [(H_A/H) + \cos\theta]^{-1}, \quad (2)$$

where  $\theta$  is the angle between  $\mathbf{H}$  and the  $c$  axis. The anisotropy field  $H_A$  is given by  $2K/M$ , where  $K$  is the relevant uniaxial anisotropy constant and  $M$  is the magnetization. Equation (2) is a good representation of the angular variations shown in Fig. 2. From fitting this curve, we obtain a value for the  $bc$  plane anisotropy field which is in excellent agreement with other experiments and also with our dipole calculation.

### C. Temperature Dependence

The thermal dependence of the magnetic moments at finite fields of stoichiometric variants of MEGIO is represented in Fig. 3. In general, all the curves, including that of the aluminum-containing sample, follow a simple monotonic Brillouin-like curve. As would be expected, the high-temperature magnetic moments at finite field do not drop sharply to zero but rather tend

<sup>10</sup> M. A. Gilleo and S. Geller, Phys. Rev. **110**, 73 (1958).

<sup>11</sup> C. H. Nowlin, Scientific Report No. 7 (Ser. 2), Cruft Laboratory, Harvard University, 1963 (unpublished).

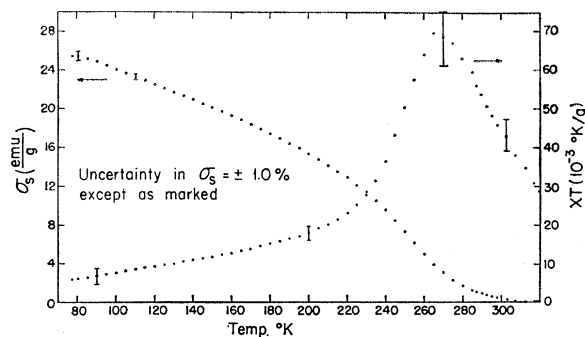


FIG. 5. Spontaneous moment and susceptibility-temperature product along the  $c$  axis of  $\text{Ga}_{0.81}\text{Al}_{0.11}\text{Fe}_{1.08}\text{O}_3$ .

to “tail off” and approach the axis asymptotically as a result of susceptibility effects. As a common rule of thumb, the inflection point of the finite-field magnetization curve is often taken as the Curie temperature. Even though this rule lacks any rigorous theoretical justification we have used it as one method of ordering the Curie temperatures of our samples in Table III.

Figures 4 and 5 show, for  $\text{Ga}_{1.14}\text{Fe}_{0.86}\text{O}_3$  and  $\text{Ga}_{0.81}\text{Al}_{0.11}\text{Fe}_{1.08}\text{O}_3$ , the thermal variation in the extrapolated zero-field moment as determined by fit to Eq. (1). These curves again show a broad high-temperature “tail off” and no ordering temperature is discernible. Belov<sup>12</sup> has pointed out that extrapolated moment provides a completely inadequate measure of long-range order in the

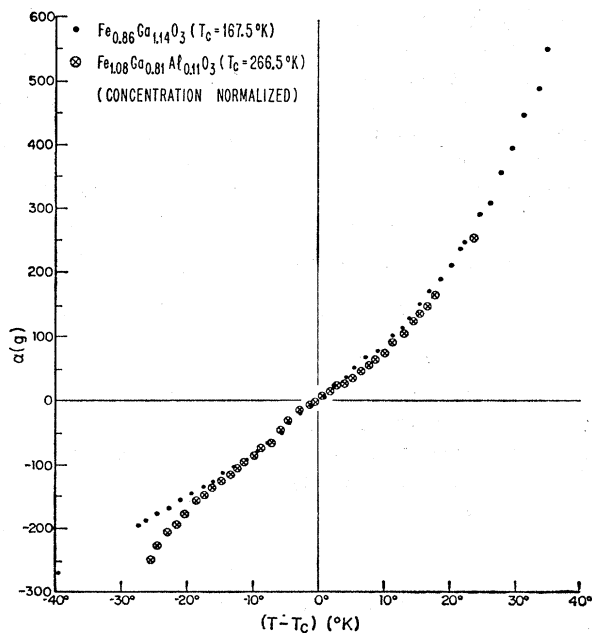


FIG. 6. Plot of thermodynamic parameter  $\alpha$  versus deviation from Curie temperature.

<sup>12</sup> K. P. Belov, *Magnetic Transitions* (Consultants Bureau Enterprises, Inc., New York, 1961).

vicinity of the critical point where the susceptibility becomes field-dependent. As a means of circumventing this difficulty, Belov and his co-workers have used extensively the so-called method of thermodynamic parameters as an extrapolation scheme for determining Curie temperatures in a variety of magnetic materials including ferrimagnetic substances. According to Landau's theory of second-order phase transitions, near  $T_c$  the field dependence of the total magnetic moment  $\sigma$  (induced + spontaneous), may be expressed as

$$\alpha + \beta\sigma^2 = H/\sigma.$$

The “thermodynamic parameters”  $\alpha$  and  $\beta$  are determined quite precisely from plots of  $\sigma^2$  versus  $H/\sigma$ . Within the context of the Landau theory, the zero of  $\alpha$  should represent the ordering temperature. Figure 6 shows the  $\alpha$  parameters derived for the two test sam-

TABLE II. Various determinations of the magnetic-ordering temperatures. Parentheses indicate that the value is not as accurate as the others.

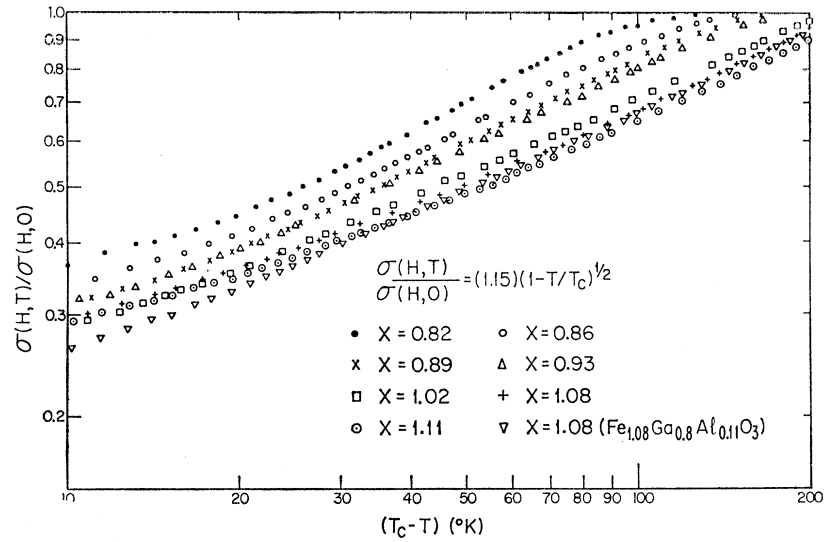
$\alpha$ for $\text{Ga}_{2-x}\text{Fe}_x\text{O}_3$	Methods of thermodynamic parameters	Inflection point ( $^{\circ}\text{K}$ )	$(d(\chi T)/dT)_{\text{max}}$ point ( $^{\circ}\text{K}$ )	Characteristic curve fit ( $^{\circ}\text{K}$ )
0.82	(135)	129	...	131
0.86	167.5	166	171	168
0.89	...	182	...	177
0.93	(184)	196	...	191
1.02	(234)	243	...	237
1.08	...	267	...	267
1.08	266.5	270	265	267
		( $\text{Ga}_{0.81}\text{Al}_{0.11}\text{Fe}_{1.08}\text{O}_3$ )		
1.11	...	295	...	285

ples. It may be seen that the two samples have essentially identical temperature dependencies near the ordering point. The quality of the data is not sufficient to fix this dependence with any precision. However, the zero-field inverse susceptibility, i.e.,  $\alpha$  above  $T_c$ , does follow a law  $(T - T_c)^{1.3 \pm 0.1}$  over a range of at least 50 K above  $T_c$ . This result is suggestive of the power-law results found in a number of simpler magnetic systems and gives us some confidence in the validity of the thermodynamic approach. It is also somewhat reassuring to note in Table II that the Curie points determined by the inflection-point rule agree within 1% with the values given by the method of thermodynamic parameters. As indicated in Fig. 4, a thermodynamic redetermination of the spontaneous moment shows no sign of a high-temperature tail off.

Further confirmation of our Curie-point determinations is obtained from the consideration of the thermal variation in the finite-field values of the product  $\chi T$  shown in Figs. 4 and 5. According to the ideas of Fisher,<sup>13</sup>

<sup>13</sup> E. M. Fisher, *Phil. Mag.* 7, 1731 (1963).

FIG. 7. Plot showing that the reduced magnetization scales with the reduced temperature according to the  $x$ -independent formula given above.



near the critical point the zero-field values of  $\chi T$  are a measure of the magnetic configurational energy of any antiferromagnetic system. Thus, the true ordering temperature should be given by the condition  $d(\chi T)/dT = \infty$ . The extension of Fisher's analysis to a ferrimagnet is by no means a trivial affair. However, in any dominantly antiferromagnetic system at finite field there is a change of state or magnetic alignment at the ordering temperature. At this point one would expect a peak in the magnetic specific heat that remains proportional to  $d(\chi T)/dT$ . It is, thus, reasonable that the maximum value of this quantity should define the ordering point at finite field. This finite-field point should be shifted up slightly from the zero-field critical temperature. From Table II we see that Curie temperatures determined from  $(d(\chi T)/dT)_{\text{max}}$  agree with those determined earlier to within 2%.

Finally, we have used the similarity of all of the curves of Fig. 4 as a further means of obtaining the Curie temperatures of our samples. It is seen in Fig. 7 that the reduced magnetization of all samples follows a curve

$$\sigma(H, T)/\sigma(H, 0) = 1.15(1 - T/T_c)^{1/2} \quad (3)$$

over a considerable range with good precision. Thus, a simple scaling of the reduced magnetization gives us the estimates of  $T_c$  listed in Table II.

One further characteristic of the behavior of the data in Figs. 4 and 5 should be mentioned. For both samples the low-temperature susceptibility is essentially temperature-independent. However, for the  $x=0.86$  sample a small paramagnetic  $T^{-1}$  contribution becomes evident at very low (helium) temperatures. Unfortunately, helium-temperature data are not available for the Al-containing sample. Up to  $\frac{1}{3}T_c$ , the suscepti-

bilities of the two samples are given by

$$\begin{aligned} x=0.86 & \quad \chi = (4.05 + 6.5/T) \times 10^{-5} \text{ g}^{-1}, \\ x=1.08 & \quad \chi = 8.08 \times 10^{-5} \text{ g}^{-1}. \end{aligned} \quad (4)$$

The temperature-independent terms are directly proportional to the low-temperature magnetic moments of the two samples, suggesting that perhaps the susceptibility arises from some small noncollinearity in the basic spin arrangement of this material.

#### D. Heat Treatment

Disordered occupation of metal sites was anticipated by Wood<sup>3</sup> on the basis of the fact that the iron-to-gallium ratio in this compound can be varied over a wide range without changing the essential crystal properties [e.g., Eq. (3)]. Thus one might expect the magnetic moment to be dependent on the thermal history of the sample. Such has been found to be the case, but the ferromagnetic Curie temperature is apparently independent of the thermal history.

MEGIO samples were held at various fixed elevated temperatures for 15-min intervals. Some of the samples were then quenched by dropping them into a cold platinum crucible while others were quenched by dropping them into oil. The results for both methods are essentially the same, and a comparison of the finite-field (approximately 6000 Oe) moments before and after quenching is shown in Fig. 8. The abscissa of Fig. 8, which is labeled "furnace temperature," gives the temperature of the sample just prior to quenching, with the exception of one point, which indicates the result of submitting the sample to the special heat treatment described below. The MEGIO magnetic

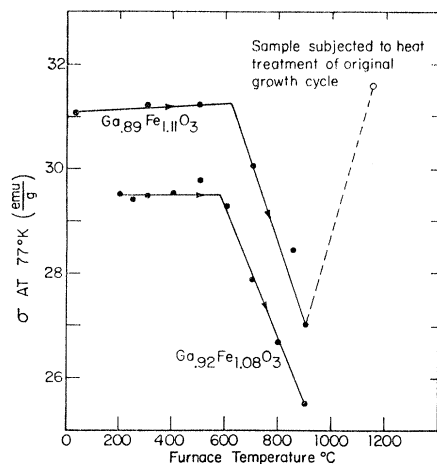


FIG. 8. Dependence of magnetic moment, measured at 77°K, on thermal history.

moment can, in general, be reduced by as much as 15% by quenching from 900°C.

Because of the relatively large difference in the x-ray scattering factors of aluminum and iron, it is possible to gather some information regarding lattice occupancy in the aluminum-containing compounds by a study of their rotating-sample x-ray diffraction photographs. It was observed that the reduction in magnetic moment was associated with the disappearance of a set of x-ray superlattice lines. This combination of phenomena indicates that the reduction in magnetic moment is indeed caused by atomic migration, rather than by chemical change.

Considerable effort was made to discover ways of restoring the original magnetic moment, which had existed prior to the quenching described above. However, the only way we were able to reattain the original magnetic moment was to subject the sample to the heat treatment of the original growth cycle, i.e., to lower the temperature slowly from about 1150°C to approximately 500°C over a 7-day period. The results of this measurement are also shown in Fig. 8.

It should be noted that the magnetic moment of the sample after this ordering treatment is about 1.5% greater than was the initial moment. This increase indicates that the sample may have become somewhat disordered by remaining at room temperature during the interval of four months between the original growth cycle and the first magnetic-moment measurement.

A similar reduction in the magnetic moment has been observed in connection with another sample. A striking feature of the data in Fig. 4 is the discontinuity, occurring at the temperature of liquid nitrogen, in the spontaneous magnetization curve. The data from the temperature of liquid nitrogen to room temperature were taken when the sample was fresh from the oven and well ordered. Then the sample was stored at room

temperature while measurements were made on other crystals. Three months later it was decided to take spontaneous-moment data from the temperature of liquid helium to that of liquid nitrogen. A reduction of 2% in the magnetic moment was discovered to have occurred during this time. The above two observations seem to indicate that the oven-fresh sample has the maximum possible magnetic moment and that a reduction of approximately 2% in the magnetic moment will take place as a result of aging at room temperature for a few months.

### III. INTERPRETATION

The complete crystal structure of the MEGIO phase has been determined by Abrahams<sup>5</sup> and co-workers in an intensive x-ray investigation. Their conclusions are confirmed by the work of Bertaut<sup>6,7</sup> and his co-workers. The oxygens are arrayed in a *double* hexagonal close-packed structure. Each unit cell contains four inequivalent cation positions which are labeled in Bertaut's notation as Fe 1, Fe 2, Ga 1, and Ga 2. The nearest-neighbor oxygens form a nearly regular tetrahedral environment about the Ga 2 site. The other sites have distorted octahedral environments. In view of the overwhelming tetrahedral site preference of Ga<sup>3+</sup>, it would be expected that the Ga 2 site would be dominantly populated by gallium ions. This expectation is indeed confirmed by the x-ray work and, as we shall see later, by the magnetic analysis.

There has been considerable discussion of the magnetic structure of MEGIO. A number of authors have conjectured a canted-spin structure for the material. However, the neutron diffraction results of Bertaut<sup>6,7</sup> and high-field Mössbauer studies by Frankel<sup>8</sup> rule out this possibility and establish the structure as a collinear ferrimagnet. In this section we show that the magnetic properties discussed in Sec. II are consistent with the collinear magnetic structure. Bertaut indexes his neutron diffraction results on basis of a four-sublattice model where each inequivalent cation site constitutes a single sublattice. He designates the sublattices 1, 2, 3, 4 for, respectively, the Fe 1, Fe 2, Ga 1, and Ga 2 sites. The sublattices 1 and 3 are antiparallel to the sublattices 2 and 4. The fractional substitution of iron ions on each type of site,  $k_i$ , must satisfy the relationship

$$k_1 + k_2 + k_3 + k_4 = 2x \quad (5)$$

for any given composition  $\text{Ga}_{2-x}\text{Fe}_x\text{O}_3$ . We may make several assumptions to determine the values of the  $k_i$ 's as functions of  $x$ . Both the neutron and x-ray results indicate that the tetrahedral substitutional parameter  $k_4$  is extremely small and may be neglected. Since the MEGIO can only be grown for  $0.7 \leq x \leq 1.4$ , it seems reasonable to say that, at the lowest iron concentration, the Ga 1 site is full of Ga<sup>3+</sup> ions (i.e.,  $k_3 = 0$  at  $x = 0.7$ ) and, furthermore, that, at the highest iron

concentration, the Fe 1 and Fe 2 sites are full of  $\text{Fe}^{3+}$  ions (i.e.,  $k_1 = k_2 = 1.0$  at  $x = 1.4$ ). Finally, Bertaut finds that the Fe 1 and Fe 2 sites are almost equally occupied, and so we set  $k_1 = k_2$ . If we suppose that concentration variations in the  $k_i$ 's are linear, then we have sufficient information to establish the relationships

$$\begin{aligned} k_1 &= k_2 = 0.43x + 0.40, \\ k_3 &= 1.14x - 0.80, \\ k_4 &= 0. \end{aligned} \quad (6)$$

As may be seen in Table III, our predictions for the  $k_i$ 's at  $x = 1.15$  agree very well with Bertaut's interpretation of neutron results at this composition. The agreement with recent neutron measurements by Delapalme<sup>14</sup> is reasonable but not as good. However, Delapalme's values do not appear consistent with his measured net magnetization and therefore are somewhat less reliable.

Using these relations for the  $k_i$ 's, we now proceed to an interpretation of the stoichiometric variations of the spontaneous moment and Curie temperature in terms of a statistical model first used by Gilleo.<sup>15</sup> This model represents a sort of first-order treatment of the complicated problem of accounting for the magnetic properties of alloy systems. In contrast with the methods of Smart,<sup>16</sup> Elliott,<sup>17</sup> and Sato,<sup>18</sup> Gilleo's model does not include correlation effects. However, the relative simplicity of the application of the model to even rather complicated multisublattice systems makes it attractive in spite of its inherent limitations.

According to Gilleo's model,<sup>15</sup> in order to calculate the spontaneous moment we must know the fraction  $(1 - E)$  of the iron ions which are magnetically *effective*. The effective ions are those with, say, two or more superexchange linkages to neighboring iron ions. The probability of having exactly  $m$  linkages between ions surrounded by  $n$  nearest neighbors is given by

$$P_n(m) = \binom{n}{m} (1-k)^{n-m} k^m, \quad (7)$$

where it is assumed that each linkage has a probability

TABLE III. Comparison between Bertaut's neutron determination of fractional iron occupation and our calculated value for  $x = 1.15$ .

	$k_1$	$k_2$	$k_3$	$k_4$
Bertaut	0.90	0.87	0.54	<0.04
Present work	0.89	0.89	0.51	0

<sup>14</sup> A. Delapalme, J. Phys. Chem. Solids **28**, 1451 (1967).

<sup>15</sup> M. A. Gilleo, J. Phys. Chem. Solids **13**, 33 (1960).

<sup>16</sup> J. S. Smart, J. Phys. Chem. Solids **16**, 169 (1960).

<sup>17</sup> R. J. Elliott, J. Phys. Chem. Solids **16**, 165 (1960).

<sup>18</sup> H. Sato, A. Arrott, and R. Kikuchi, J. Phys. Chem. Solids **10**, 19 (1959).

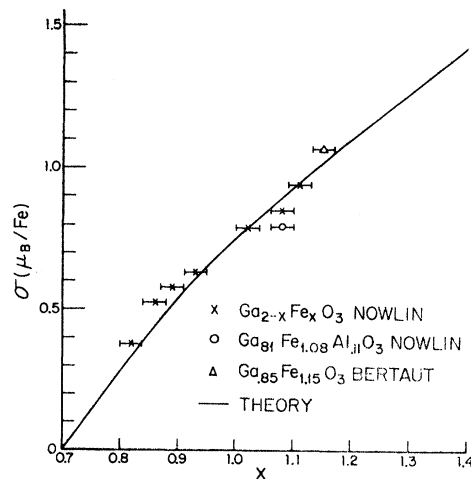


FIG. 9. Comparison between theory (with no adjustable parameters) and experiment for the variation of spontaneous moment with iron concentration.

$k$ . Thus, the probability that a given iron ion is surrounded by none or at most one linkage is

$$\begin{aligned} E &= P_n(0) + P_n(1) \\ &= n(1-k)^{n-1} - (n-1)(1-k)^n. \end{aligned} \quad (8)$$

Each of the Fe 1, Fe 2, and Ga 1 sites has one  $180^\circ$  superexchange bond. In addition, there are several  $120^\circ$  bonds and others distributed between  $90^\circ$  and  $120^\circ$ . It is, thus, difficult to rigorously assess the value  $n$  to be used in Eq. (8). However, at low  $x$ , where the Ga 1 iron concentration is small, a value  $n = 3$  seems reasonable for each site. Since  $E$  is a small correction term of the order of 10% ( $x \approx 1$ ) and considering the approximate nature of the Gilleo model, the value of  $n$  is not critical and further refinements seem unwarranted. Using our result for  $k_1$ , we obtain a value for  $E$  at  $x = 0.7$ . If we assume that  $E$  decreases linearly to zero at  $x = 1.4$ , we find

$$E = 0.44 - 0.314x. \quad (9)$$

The assumed linearity of  $E$  has made it the same for all sites. The total net spontaneous magnetization, in Bohr magnetons per ferric ion (arising from the moment on Ga 1 site), may be obtained without benefit of any adjustable parameters as

$$\sigma = (5/2x)(1-E)k_3. \quad (10)$$

Figure 9 shows that this relation fits the experimental data quite well. It will be also noted in Fig. 9 that the  $\text{Al}^{3+}$ -containing sample falls below the pure  $\text{Ga}^{3+}$  samples. This indicates that the  $\text{Al}^{3+}$  ions have a greater preference for the Ga 1 site.

Bertaut<sup>7</sup> and Delapalme<sup>14</sup> note that neutron magnetic scattering amplitudes at  $x = 1.15$  indicate reduced average moments of  $(4.0 \pm 0.5)\mu_B$  and  $(4.8 \pm 0.07)\mu_B$ ,

respectively, associated with each site. We attribute this reduction to a decrease in the number of statistically effective moments, so that  $\bar{\mu} = 5(1-E)\mu_B = 4.6\mu_B$ .

A further indication of the essential correctness of the statistical approach is found by considering the low-temperature susceptibility data of the  $x=0.86$  sample. As mentioned earlier the data exhibit a small paramagnetic  $T^{-1}$  contribution, which can be explained if about  $\frac{1}{2}\%$  of the total number of ferric ions are paramagnetic. This assumption is certainly consistent with the statistical model which predicts that 1% of the moments should be free, i.e.,  $P_n(0) = (1-k_1)^3 = (0.23)^3$ .

It has been found<sup>15,19</sup> that the Curie temperature of iron oxides is determined by the number  $\nu$  of superexchange linkages per  $\text{Fe}^{3+}$  ion per formula unit. A large number of compounds for which  $\text{Fe}^{3+}$  is the only magnetic ion have values of  $T_c/\nu$  ranging from 106 to 132°K. The exact value depending on the superexchange angle and the distance between  $\text{Fe}^{3+}$  ions.

If  $n$  is the number of active superexchange linkages per formula unit and  $N$  is the number of active magnetic ions that contribute towards ferromagnetism per formula unit, then

$$\nu = n/N. \quad (11)$$

As before, taking all sites to have three iron nearest neighbors, each with probability  $k_1$ , and including the additional 180° Fe 1-O-Ga 1 bond for site 1, which becomes important for large  $x$ , we obtain

$$n = \frac{1}{2}[6k_1^2(1-E)^2 + 4k_1k_3(1-E)^2], \quad (12)$$

$$N = (1-E)x, \quad (13)$$

$$\nu = [(1-E)k_1/x][3k_1 + 2k_3]. \quad (14)$$

Taking  $T_c/\nu = 100^\circ$  for MEGIO, together with Eq. (14) completely determines the Curie temperature as a function of  $x$ . It is seen in Fig. 10 that this calculation is in reasonable agreement with the various determinations of  $T_c$ . Mössbauer experiments by Trooster<sup>20</sup> give somewhat lower values for  $T_c$  than these determinations.

#### IV. DIPOLAR ANISOTROPY CALCULATION

Since the crystal field in MEGIO is not strong,<sup>21</sup> the  $\text{Fe}^{3+}$  ion in MEGIO is in a high-spin  $S$  state, and it has been difficult to understand the origin of the large anisotropy energy. We have done a calculation of the classical dipole energy and find that this interaction accounts very well for the sign, magnitude, temperature variation and iron concentration dependence of the measured anisotropy constants. It is not surprising that

the dipolar anisotropy is so large, since MEGIO is highly noncubic and has a magnetic structure consisting of alternating sheets of spins with each sheet perpendicular to the  $b$  axis. All the spins in any one sheet are parallel to each other but are antiparallel to all the spins in the neighboring sheets.

Using the molecular-field approximation we can express the dipolar energy as

$$U = \frac{1}{2} \sum_{\mu, \nu} \sum_{m, n} (M_m)_\mu \Phi_{mn}^{\mu\nu} [(M_n)_\nu / N_n], \quad (15)$$

where  $(M_n)_\nu$  is the  $\nu$  component of the magnetization of sublattice  $n$ ,  $N_n$  is the number of atoms per  $\text{cm}^3$  on sublattice  $n$ , and the symmetric tensor  $\Phi$  is given by

$$\Phi_{mn}^{\mu\nu} = \Phi_{nm}^{\mu\nu} = \sum_j \frac{1}{r_{ij}^3} \left( 1 - \frac{3(r_{ij})_\mu (r_{ij})_\nu}{r_{ij}^2} \right). \quad (16)$$

$(r_{ij})_\mu$  is the  $\mu$  component of the distance between the  $i$  and  $j$  atomic sites. In order to evaluate  $\Phi$ , we choose an origin on atom  $i$  of sublattice  $m$  and sum  $j$  over all the atoms on sublattice  $n$ .

The advantage of this approach is that both the temperature dependence and the iron concentration dependence of the dipolar interaction has been factored out of  $\Phi$ , which can be determined once and for all. Then the variation of the anisotropy energy with temperature and  $x$  can easily be evaluated by hand.

$\Phi$  was calculated on a computer by summing  $j$  over a sphere having a volume of 5800 unit cells. This sum was also done for a smaller sphere of 4100 unit cells in order to check convergence. Abrahams's<sup>5</sup> atomic coordinates were used.

For orthorhombic symmetry the anisotropy energy has the form

$$U = K_1\alpha_1^2 + K_2\alpha_2^2 + K_3\alpha_3^2, \quad (17)$$

- { THERMODYNAMIC PARAMETERS,  
INFLECTION POINT, AND  
CHARACTERISTIC CURVE
- △ FRANKEL
- BERTAUT

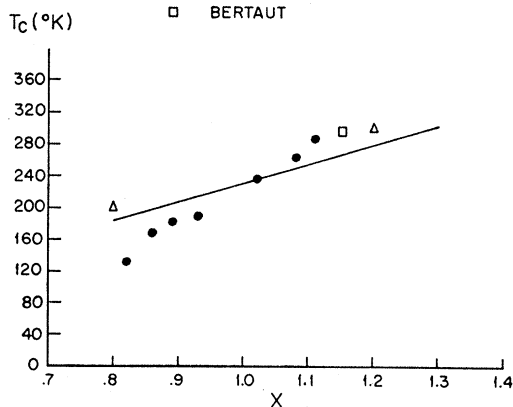


FIG. 10. Comparison between theory and experiment for dependence of Curie temperature on iron concentration.

<sup>19</sup> M. A. Gilleo, Phys. Rev. **109**, 777 (1958).

<sup>20</sup> J. M. Trooster and A. Dymanus, Phys. Status Solidi **24**, 487 (1967).

<sup>21</sup> R. V. Pisarev, Fiz. Tverd. Tela **7**, 207 (1965) [English transl.: Soviet Phys.—Solid State **7**, 158 (1965)].

where the direction cosines  $\alpha_1, \alpha_2, \alpha_3$  refer to the angle between the net magnetization and the  $a, b,$  and  $c$  axes, respectively.

By comparing Eqs. (15) and (17), we can express the anisotropy constants  $K_i$  in terms of the tensor  $\Phi$ . Figure 11 shows the resulting  $\text{Fe}^{3+}$  concentration dependence of the anisotropy constants  $K_a = K_1 - K_3$  and  $K_b = K_2 - K_3$ , which are appropriate for rotation in the  $ac$  plane and  $bc$  plane, respectively.

Figure 12 shows the calculated anisotropy fields  $H_a$  and  $H_b$  as a function of  $x$ . It is to be noted that  $H_b$  is quite large, increasing from 43 kOe at  $x=1.4$  to 150 kOe at  $x=0.8$ . The anisotropy constants  $K_a$  and  $K_b$  increase with increasing  $x$  as expected. The unusual increase of the anisotropy fields  $H_{a,b} = 2K_{a,b}/M$  with decreasing  $x$  results from the total magnetization  $M$  (due almost entirely to the rapidly varying moment on sublattice 3) decreasing faster than  $K$  which has contributions from all three sublattices.

Pinto<sup>22</sup> has measured the anisotropy constants using a torque method on a sample for which  $x \approx 1.11$ ; Dweck<sup>23</sup> has done FMR also on a  $x=1.1$  crystal obtaining the same anisotropy values; and Dymanus and Kaminow,<sup>24</sup> using FMR, measured them for  $x \approx 1.3$ . The closeness between our calculated values and these measurements is demonstrated in Fig. 12. The excellent agreement between Pinto's  $K_b$  measured at  $77^\circ$  but renormalized for  $T=0$  ( $5.26 \times 10^6$  erg/cm<sup>3</sup>) and the value calculated for  $x=1.10$  ( $5.24 \times 10^6$  erg/cm<sup>3</sup>) is well within the possible 2% variation caused by the uncertainty in the known value for  $x$ . Thus the dipolar interaction

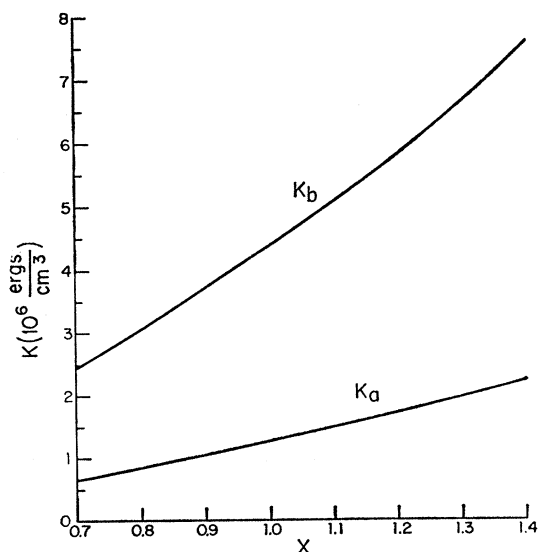


FIG. 11. Calculated dipolar anisotropy constants as a function of iron concentration.

<sup>22</sup> A. Pinto, J. Appl. Phys. **37**, 4372 (1966).

<sup>23</sup> J. Dweck, Phys. Rev. **168**, 602 (1968).

<sup>24</sup> A. Dymanus and I. P. Kaminow, J. Appl. Phys., Suppl. **32**, 144S (1961).

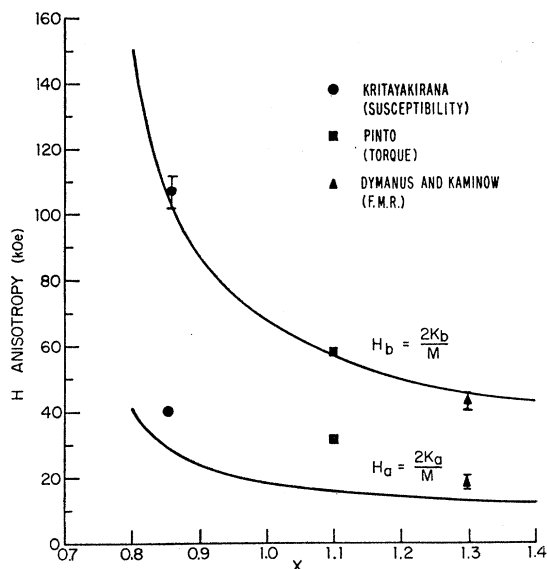


FIG. 12. Comparison of calculated low-temperature dipolar anisotropy fields and experimental values as a function of iron concentration. The measurements of Pinto, and Dymanus and Kaminow have been renormalized to be appropriate for  $T=0^\circ\text{K}$  by assuming  $K(T) \propto M(T)^2$ . The error bars on the latter are due to the uncertainty introduced in renormalizing their room-temperature data.

completely accounts for the large anisotropy in the  $bc$  plane.

To confirm the large predicted rise in the anisotropy field at low  $x$ , we measured the rotation curve shown in Fig. 2. From this curve we find that, for  $x=0.86$ ,  $H_b = 107 \pm 5$  kG. This is in excellent agreement with the calculated value of 104 kG, as shown in Fig. 12.

In an attempt to determine whether dipolar forces could account for the additional contribution to the  $ac$  plane anisotropy, the atomic coordinates were varied by a few percent, but this only modified the  $K_i$  a few percent. Nor can a slight canting of the sublattices from collinearity explain the discrepancy.

This additional anisotropy is therefore a spin-orbit effect. This conclusion is supported by the strong magnetoelectric effect, which is too large to be explained by combining the piezoelectric effect with the purely dipolar magnetoelastic constants which we calculate in the next section. Furthermore, the deviation of the  $g$  factor from 2, as observed in FMR,<sup>23,24</sup> suggests that anisotropic exchange effects are not negligible and in fact may be roughly of the order of magnitude needed to explain the additional  $ac$  plane anisotropy. If this anisotropic exchange has the pseudodipolar form, then it would explain (see following paragraphs) Pinto's<sup>22</sup> experimental result that the temperature dependence of both  $K_a$  and  $K_b$  is given by  $M^2$ . In view of the preceding comments, it is perhaps somewhat surprising that the fit between the measured and dipolar  $K_b$  is virtually perfect.

TABLE IV. Three-sublattice molecular-field coefficients.

$\lambda_{23} = -10\,750$
$\lambda_{13} = -6850$
$\lambda_{12} = -5760$
$\lambda_{22} = -5050$
$\lambda_{33} = -1820$
$\lambda_{11} = -504$

In order to determine the variation of the anisotropy constants with temperature, we need the individual sublattice magnetizations. To obtain this we did a computer fit<sup>25</sup> to the measured net magnetization for the composition  $x=0.86$ . The data for this fit were obtained by renormalizing Fig. 4 to eliminate the artificial break at 77°K. Near the Curie temperature the thermodynamic redetermination of the spontaneous moment was used. The temperature coefficient of the molecular-field constants ( $-0.8 \times 10^{-4} \text{ }^\circ\text{K}^{-1}$ ) was taken from Bertaut.<sup>7</sup>

We used a three-sublattice model since the tetrahedral gallium site is virtually devoid of iron. The deviation of the calculated net magnetization from the measured value was less than 1% of the spontaneous moment of sublattice 1 (Fe 1) or 2 (Fe 2). We did not attempt to fit the curve any better for the following reasons. The low-temperature sublattice magnetizations are only known to a few percent, due partly to the uncertainty in the measured value for  $x$ ; we have neglected the very small but finite contribution of the tetrahedral gallium site to the moment; and the magnetization obtained by the method of thermodynamic parameters may be in error by 1 or 2%.

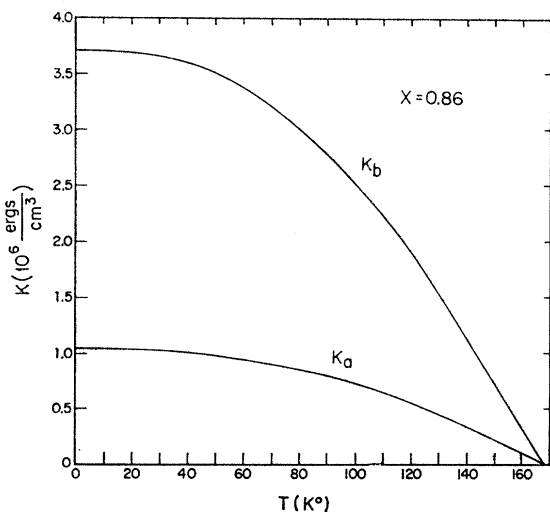


FIG. 13. Temperature dependence of calculated dipolar anisotropy constants.

<sup>25</sup> G. Heiche, U.S. Naval Ordnance Laboratory Technical Report 63-32, 1964 (unpublished).

The resulting molecular-field coefficients  $\lambda_{ij}$ , defined by  $H_i = \lambda_{ij} M_j$ , are displayed in Table IV. As expected,  $\lambda_{11}$  is small since the Fe 1-Fe 1 distance is much larger than any of the other inter- or intrasublattice distances.

The temperature dependences of the three sublattices are nearly the same, and hence the net magnetization follows this same temperature variation. Consequently, Eq. (15) shows that  $K$  is approximately proportional to  $M^2$ , as Pinto<sup>22</sup> determined experimentally for  $x=1.1$ . Figure 13 shows  $K_a$  and  $K_b$  as a function of temperature for  $x=0.86$ . The straight-line region heading in towards the Curie temperature is simply a result of  $K \propto M^2$ .

Since dipolar forces are so large, it is interesting to calculate their contribution to the magnetoelastic constants. These  $B_{ijkl}$  may be obtained from the strain ( $e_{kl}$ ) induced variation in the anisotropy energy given by Eq. (15):

$$B_{ijkl} = \partial^2 U / \partial \alpha_i \partial \alpha_j \partial e_{kl}. \quad (18)$$

The differentiation was evaluated algebraically (see

TABLE V. Dipolar magnetoelastic tensor in units of  $10^6 \text{ erg/cm}^3$ .

$B_{1111} \equiv B_{11} = 3.0$
$B_{2222} \equiv B_{22} = 6.3$
$B_{3333} \equiv B_{33} = 14.6$
$B_{2323} \equiv B_{44} = 11.3$
$B_{1313} \equiv B_{55} = -13.8$
$B_{1212} \equiv B_{66} = -10.4$
$B_{1122} \equiv B_{12} = B_{21} = -3.6$
$B_{1133} \equiv B_{13} = B_{31} = -3.8$
$B_{2233} \equiv B_{23} = B_{32} = 11.9$

Appendix) so that the computer did not have to take small differences between large numbers. For simplicity the  $B$ 's were calculated at  $T=0$  for all three sublattices completely full of iron, slightly overestimating the values appropriate for  $x=1.4$ . The nonvanishing  $B$ 's for orthorhombic symmetry are listed in Table V. As  $x$  decreases the  $B$ 's also decrease, similar to the behavior of  $K_a$  and  $K_b$  in Fig. 11.

The  $\text{Fe}^{3+}$  ion in YIG is also in an  $S$  state, but its cubic symmetry means that dipolar effects are very small. Thus it is of interest to compare  $B_1 = 3 \times 10^6 \text{ erg/cm}^3$  and  $B_2 = 12 \times 10^6 \text{ erg/cm}^3$  at  $T=0$ <sup>26</sup> with the above. This comparison suggests that there may be nondipolar contributions to the  $B$ 's in MEGIO. Experiments are now under way to measure these magnetoelastic constants in order to determine the importance of spin-orbit effects and perhaps shed some light on the extra  $ac$  plane anisotropy mechanism.

The large anisotropy produces interesting domain-wall structures as shown in Figs. 14 and 15. These were

<sup>26</sup> P. J. Flanders, R. F. Pearson, and J. L. Page, Brit. J. Appl. Phys. 17, 839 (1966).

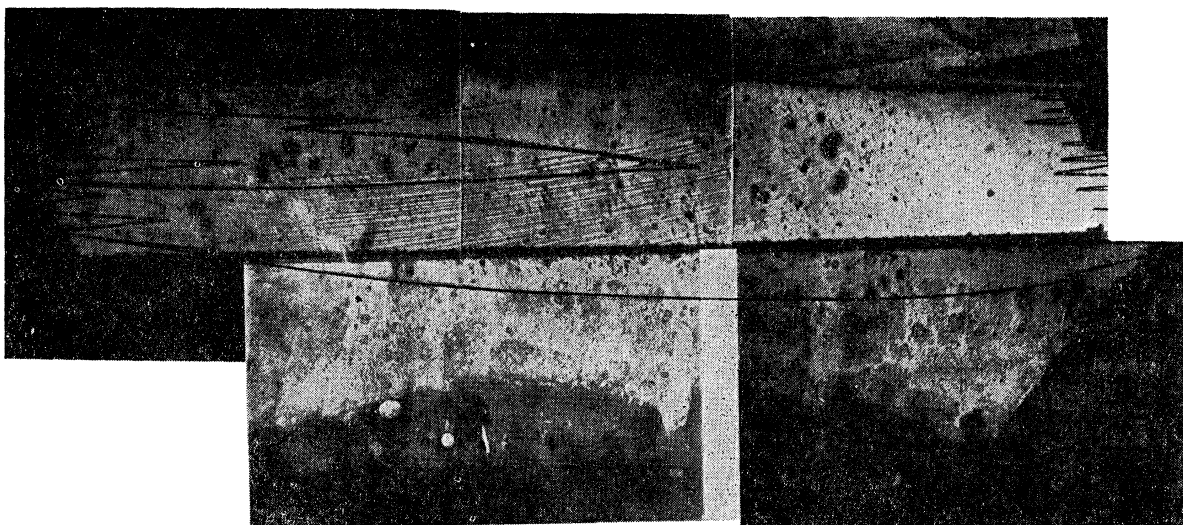


FIG. 14. Composite photographs of domain-wall Bitter patterns. The  $c$  axis is horizontal (along length of rod). The three pictures on the left are one crystal surface while the two on the right are another surface perpendicular to it. (Retouched).

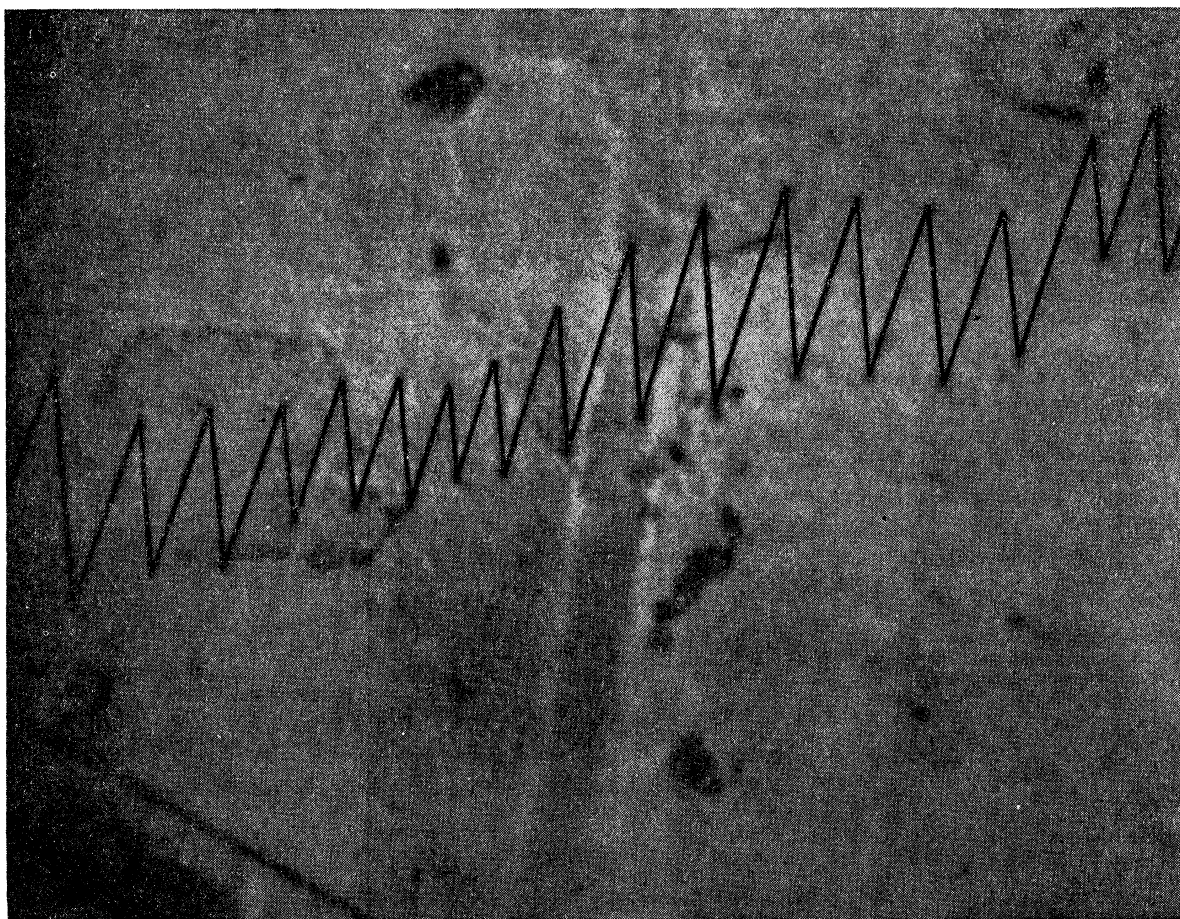


FIG. 15. Zig-zag domain-wall boundary.  $c$  axis vertical. (Retouched.)

obtained by the usual Bitter pattern technique. In Fig. 14 two perpendicular surfaces of the crystal are juxtaposed. Note the domain wall which runs from the right to the left on the bottom surface and then continues around the corner a short distance to the edge of the other surface. This indicates that these domain walls are a bulk phenomenon and not merely a surface effect. Note also the sharp domain closure spikes at the ends of the rod in Fig. 14. Similar domain closure spikes and zig-zag walls are seen in high uniaxial anisotropy materials such as cobalt.<sup>27</sup>

## V. CONCLUSIONS

Using a three-sublattice collinear ferrimagnetic model and making reasonable assumptions concerning the iron and gallium site preferences, we have determined the fractional iron occupation as a function of  $x$  for all sites  $k_i(x)$  in very good agreement with neutron results. Without any adjustable parameters we use these  $k_i(x)$  and a simple statistical model to calculate the net spontaneous magnetization as a function of  $x$ , obtaining close agreement with our measurements.

Again employing this statistical model we calculate the small fraction of isolated paramagnetic spins and find agreement with our low-temperature susceptibility measurements. A further check on this model is its explanation of the reduced average moment per atom, which is observed in neutron experiments.

A molecular-field computation of the classical dipolar energy is in excellent agreement with the measured magnitude, sign, and  $x$  dependence of the large  $bc$  plane anisotropy constant. This close fit is a further check on the correctness of both  $k_i(x)$  and the statistical argument. The smaller  $ac$  plane anisotropy has an additional spin-orbit contribution which seems to be pseudodipolar anisotropic exchange.

The high-temperature tail on the spontaneous magnetization was eliminated using Landau's theory of second-order phase transitions and this thermodynamically redetermined magnetization used to obtain the molecular-field coefficients  $\lambda_{ij}$  and the various sublattice temperature dependences. From these results we calculated the temperature variation of the anisotropy constants and found it was given by  $K \propto M^2$ , as Pinto has measured with torque experiments.

Finally, the dipolar contribution to the magnetoelastic tensor was calculated.

## ACKNOWLEDGMENT

We wish to thank K. Kritayakirana for the magnetization rotation measurement (Fig. 2).

<sup>27</sup> D. J. Craik and R. S. Tebble, *Ferromagnetism and Ferromagnetic Domains* (John Wiley & Sons, Inc., New York, 1965).

## APPENDIX

Since the sublattices are collinear, we may set

$$(M_n)_\mu = M_n \alpha_\mu, \quad (\text{A1})$$

where  $\alpha_\mu$  is the direction cosine with the orthorhombic axes and  $M_n$  is the algebraic magnitude, which is positive or negative if it is parallel or antiparallel, respectively, to the direction of the net magnetization. Rewriting Eq. (15), we obtain

$$U = \frac{1}{2} \sum_{m,n} (M_m M_n / N_n) \sum_j [(1/r^3) - (3\alpha_p \alpha_q r_p r_q / r^5)]. \quad (\text{A2})$$

For conciseness we use the summation convention on the repeated subscripts  $p, q, s$ , and  $t$ . Furthermore, we temporarily suppress the sum on  $m, n$ , and  $j$ . The derivative of  $U$  is then

$$dU = [(15\alpha_p \alpha_q r_p r_q / r^6) - 3/r^4] dr - (6\alpha_p \alpha_q r_p dr_q / r^5). \quad (\text{A3})$$

Following Kittel's<sup>28</sup> notation, we can introduce the strain tensor  $e_{pq}$  as follows:

$$dr_p = \left(\frac{1}{2} + \frac{1}{2} \delta_{pq}\right) e_{pq} r_q, \\ dr = \left(\frac{1}{2} + \frac{1}{2} \delta_{pq}\right) (r_p e_{pq} r_q / r), \quad (\text{A4})$$

where  $\delta_{pq}$  is the Kronecker  $\delta$ .

Substituting (A4) into (A3) and comparing the result to

$$dU = B_{pqst} \alpha_p \alpha_q e_s e_t,$$

we obtain, after including the sums over  $m, n$ , and  $j$ ,

$$B_{pqst} = \frac{1}{2} \sum_{m,n} (M_m M_n / N_n) \sum_j [(15/r^7) r_p r_q r_s r_t \\ - (6/r^5) r_q r_t \delta_{ps}] \left(\frac{1}{2} + \frac{1}{2} \delta_{pq}\right).$$

All the  $B$ 's which multiply identical combinations of  $\alpha$ 's and  $e$ 's must be combined. Thus, for example,

$$B_{66} \equiv (B_{1212})_{\text{Total}} = B_{1212} + B_{1221} + B_{2121} + B_{2112}.$$

Therefore, we have

$$B_{66} = \frac{1}{2} \sum_{m,n} (M_m M_n / N_n) \sum_j [(30x^2 y^2 / r^7) \\ - (3/r^5) (x^2 + y^2)].$$

The sum over  $j$  was the quantity evaluated by computer.

<sup>28</sup> C. Kittel, *Introduction to Solid State Physics* (John Wiley & Sons, Inc., New York, 1961), p. 87.

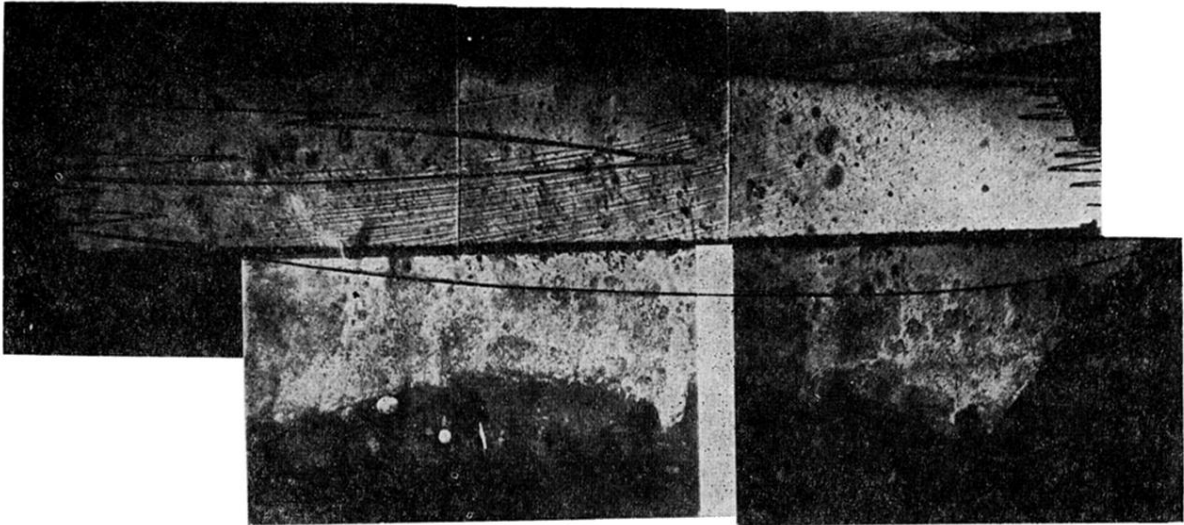


FIG. 14. Composite photographs of domain-wall Bitter patterns. The  $c$  axis is horizontal (along length of rod). The three pictures on the left are one crystal surface while the two on the right are another surface perpendicular to it. (Retouched).

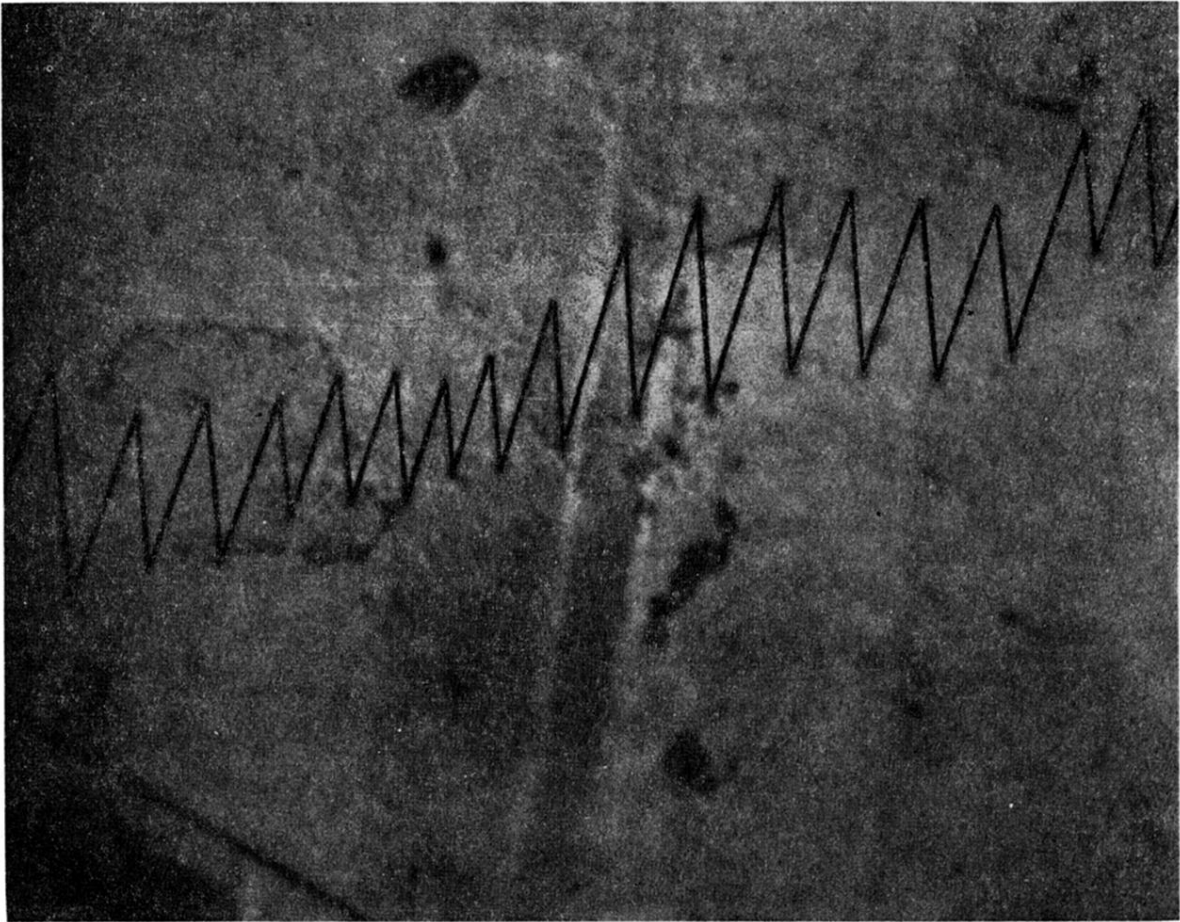


FIG. 15. Zig-zag domain-wall boundary.  $c$  axis vertical. (Retouched.)